Earth System
Dynamics
Discussions

1   # Soil frost-induced soil moisture precipitation feedback
2   # over high northern latitudes

3   **Stefan Hagemann[1*], Tanja Blome[1], Altug Ekici[2] and Christian Beer[3]**

4   [1] Max-Planck-Institut für Meteorologie, Bundesstr. 53, 20146 Hamburg, Deutschland,
5   [*] Tel.: +49 40 4117 3101, Email: stefan.hagemann@mpimet.mpg.de

6   [2] Earth System Sciences, Laver Building, University of Exeter, Exeter, UK

7   [3] Department of Environmental Science and Analytical Chemistry (ACES) and Bolin Centre
8   for Climate Research, Stockholm University, Stockholm, Sweden.

9

10

Earth System
Dynamics
Discussions

EGU

Abstract

Permafrost or perennially frozen ground is an important part of the terrestrial cryosphere; roughly one quarter of Earth's land surface is underlain by permafrost. The impact of the currently observed warming, which is projected to persist during the coming decades due to anthropogenic CO_2 input, certainly has effects for the vast permafrost areas of the high northern latitudes. The quantification of these effects, however, is scientifically still an open question. This is partly due to the complexity of the system, where several feedbacks are interacting between land and atmosphere, sometimes counterbalancing each other. Moreover, until recently, many global circulation models (GCMs) and Earth system models (ESMs) lacked the sufficient representation of cold region physical soil processes in their land surface schemes, especially of the effects of freezing and thawing of soil water for both energy and water cycles. Therefore, it will be analysed in the present study how these processes impact large-scale hydrology and climate over northern hemisphere high latitude land areas. For this analysis, the atmosphere-land part of MPI-ESM, ECHAM6-JSBACH, is driven by prescribed observed SST and sea ice in an AMIP2-type setup with and without newly implemented cold region soil processes. Results show a large improvement in the simulated discharge. On one hand this is related to an improved snowmelt peak of runoff due to frozen soil in spring. On the other hand a subsequent reduction of soil moisture leads to a positive land atmosphere feedback to precipitation over the high latitudes, which reduces the model's wet biases in precipitation and evapotranspiration during the summer. This is noteworthy as soil moisture – atmosphere feedbacks have previously not been in the research focus over the high latitudes. These results point out the importance of high latitude physical processes at the land surface for the regional climate.

Keywords: Soil moisture – precipitation feedback, soil water freezing, permafrost regions,

35   global climate modelling, high latitudes

1   Introduction

37   Roughly one quarter of the northern hemisphere terrestrial land surface is underlain by

38   permafrost (Brown et al., 1997; French, 1990), which is defined as ground that is at or below

39   zero degrees Celsius for more than two consecutive years. Permafrost soils build a globally

40   relevant carbon reservoir as they store large amounts of deep-frozen organic material with

41   high carbon contents. In recent years, estimates for the amount of carbon stored in soils have

42   attracted more and more attention, and here especially the consideration of the vast permafrost

43   regions increased numbers of these estimates drastically (Tarnocai et al., 2009; Zimov et al.,

44   2006; Schuur et al., 2008; McGuire et al., 2009). It is believed to store between 1400 and

45   1800 Pg of C in the upper few meters of the soil (Schuur et al., 2008), which would be twice

46   the amount of the atmosphere's content. The high northern latitudes are one of the critical

47   regions of anthropogenic climate change, where the observed warming is clearly above

48   average due to the so-called Arctic Amplification (Solomon et al., 2007; ACIA, 2005).

49   Climate model simulations project this trend to continue (Serreze and Barry, 2011). The

50   combination of the high C stocks in sub-arctic and arctic soils with the pronounced warming

51   in the affected regions could thus lead to a positive feedback through the release of formerly

52   trapped, 'deep-frozen' C into the atmosphere, when near-surface permafrost thaws. For the

53   thawed soils and their biogeochemistry, it is decisive whether dry or wet conditions

54   predominate: Aerobic decomposition is relatively fast and leads to the release of CO_2, while

55   anaerobic decomposition is much slower and leads to the release of CH_4 as the main product

56   of the combustion of organic soil material. CH_4 is a much more potent greenhouse gas, but

57   has a shorter lifetime of about 10 years after which it becomes CO_2. Therefore, not only the

58   soil's temperature, but also its moisture status are important for the assessment of the

59   biogeochemical response to climatic conditions, and thus should be represented in climate or

60   Earth System models in a realistic and process-based manner. Thus, the adequate

61   representation of permafrost hydrology is a necessary and challenging task in climate

62   modelling.

63   Hagemann et al. (2013a) described relevant hydrological processes that occur in permafrost

64   areas and that should preferably be represented in models simulating interactions of

65   permafrost hydrology with vegetation, climate and the carbon cycle. The current state of the

66   representation of processes in general circulation models (GCMs) or Earth system models

67   (ESMs) can be obtained by systematic model intercomparison through the various climate

68   model intercomparison projects (CMIPs; Meehl et al., 2000) that have a long history within

69   the climate modelling community. Results from CMIPs provide a good overview on the

70   respective state of ESM model accuracy and performance. Koven et al. (2012) analysed the

71   performance of ESMs from the most recent CMIP5 exercise over permafrost areas. They

72   found that the CMIP5 models have a wide range of behaviours under the current climate, with

73   many failing to agree with fundamental aspects of the observed soil thermal regime at high

74   latitudes. This large variety of results originates from a substantial range in the level of

75   complexity and advancement of permafrost-related processes implemented in the CMIP5

76   models (see, e.g., Hagemann et al., 2013a), whereat most of these models do not include

77   permafrost specific processes, not even the most basic process of freezing and melting of soil

78   water. Due to missing processes and related deficiencies of their land surface schemes,

79   climate models often show substantial biases in hydrological variables over high northern

80   latitudes (Luo et al., 2003; Swenson et al., 2012). Moreover, the land surface

81   parameterizations used in GCMs usually do not adequately resolve the soil conditions (Walsh

82   et al., 2005), which often rely on either point measurements or on information derived from

83   satellite data. Therefore, large efforts are ongoing to extend ESMs in this respect, in order to

84   improve simulated soil moisture profiles and associated ice contents, river discharge, surface

85   and sub-surface runoff. The ESM improvement over permafrost areas was, e.g., one of the

86   research objectives of the European Union Project PAGE21 (www.page21.org).

87   The most basic process in permafrost areas is the seasonal melting and freezing of soil water

88   in the presence of continuously frozen ground below a certain depth. The response of the soil

89   to freezing leads to specific variations in the annual cycle of soil hydrology. Frozen ground

90   and snow cover also influence rainfall-runoff partitioning, the timing and magnitude of spring

91   runoff, and the amount of soil moisture that subsequently is available for evapotranspiration

92   in spring and summer (Koren et al., 1999). Soil moisture controls the partitioning of the

93   available energy into latent and sensible heat flux and conditions the amount of surface

94   runoff. By controlling evapotranspiration, it is linking the energy, water and carbon fluxes

95   (Koster et al., 2004; Dirmeyer et al., 2006; Seneviratne and Stöckli, 2008). Seneviratne et al.

96   (2006) stated that a northward shift of climatic regimes in Europe due to climate change will

97   result in a new transitional climate zone between dry and wet climates with strong land–

98   atmosphere coupling in central and eastern Europe. They specifically highlight the importance

99   of soil-moisture–temperature feedbacks (in addition to soil-moisture–precipitation feedbacks)

100   for future climate changes over this region. A comprehensive review on soil moisture

101   feedbacks is given by Seneviratne et al. (2010).

102   Largely, soil moisture feedbacks to the atmosphere are confined to regions where the

103   evapotranspiration is moisture-limited. These are regions where the soil moisture is in the

104   transitional regime between the permanent wilting point (soil moisture content below which

105   the plants can not extract water from the soil by transpiration as the suction forces of the soil

106   are larger than the transpiration forces of the plants) and the critical soil moisture W_{crit} above

107   which plants transpire at the potential rate (see, e.g., Fig. 5 in Seneviratne et al., 2010). In this

108   respect, the high-latitudes are usually excluded those regions as they are considered to be

109   predominantly energy-limited (Teuling et al., 2009), and where the coupling between soil

110   moisture and the atmosphere does not play a role (Koster et al., 2004, 2006).

111   Note that in previous studies where an ESM's land surface model (LSM) was equipped with

112   cold region soil processes, effects of resulting model improvements usually have not been

113   directly considered in a coupled atmosphere-land context. Either simulated changes were only

114   considered in the LSM standalone mode (e.g. Ekici et al., 2014, 2015; Lawrence and Slater,

115   2005; Gouttevin et al., 2012; Slater et al., 1998), or changes between different LSM version

116   were not limited to cold region processes alone (Cox et al., 1999). Thus, any soil moisture

117   feedbacks to the atmosphere related to cold region soil processes have been neglected so far.

118   In the present study, we show that the implementation of cold region soil processes into the

119   ESM of the Max Planck Institute for Meteorology, MPI-ESM, has a pronounced impact on

120   the simulated terrestrial climate over the northern high latitudes, and that this is mainly related

121   to a positive soil moisture-precipitation feedback. Section 2 introduces the used ESM version

122   and the setup of the associated simulations, Section 3 discusses the main results over several

123   high latitude river catchments, followed by a summary and conclusions in Section 4.

2 Model, data and methods

2.1 Model description

126   In this study, the atmosphere and land components of the Earth System Model (ESM) of the

127   Max Planck Institute for Meteorology (MPI-M), MPI-ESM 1.1, are utilized that consist of the

128   atmospheric GCM ECHAM6.3 (Stevens et al., 2013) and its land surface scheme JSBACH

129   3.0 (Raddatz et al., 2007, Brovkin et al., 2009). Both models have undergone several further

130 developments since the version (ECHAM6.1/JSBACH 2.0) used for the Coupled Model

131 Intercomparison Project 5 (CMIP5; Taylor et al., 2012). Several bug fixes in the ECHAM

132 physical parameterizations led to energy conservation in the total parameterized physics and a

133 re-calibration of the cloud processes resulted in a medium range climate sensitivity of about 3

134 K. JSBACH 3.0 comprises several bug fixes, a new soil carbon model (Goll et al., 2015) and

135 a five layer soil hydrology scheme (Hagemann and Stacke, 2015) replaced the previous

136 bucket scheme. In addition, a permafrost-ready version of JSBACH is considered (JSBACH-

137 PF) in which physical processes relevant at high latitude land regions have been implemented

138 by Ekici et al. (2014). Most importantly, these processes comprise the freezing and melting of

139 soil moisture. Consequently, the latent heat of fusion dampens the amplitude of soil

140 temperature, infiltration is decreased when the uppermost soil layer is frozen, soil moisture is

141 bound in solid phase when frozen, and, hence, cannot be transported vertically or horizontally.

142 Dynamic soil thermal properties now depend on soil texture as well as on soil water and ice

143 contents. Dynamic soil hydraulic properties that depend on soil texture and soil water content

144 are decreased when soil moisture is frozen. Moreover a snow scheme has been implemented

145 in which snow can now develop in up to five layers while the current scheme only represents

146 up to two layers. The latter also thermally lets the snow grow inside the soil (i.e. soil

147 temperatures are mixed with snow temperatures), while the new scheme accumulates the

148 snow on top of the soil using snow thermal properties. Further, a homogeneous organic top

149 layer is added with a constant depth and specific thermal and hydraulic properties.

150 **2.2 Experimental setup**

151 Two ECHAM6.3/JSBACH simulations were conducted at T63 horizontal resolution (about

152 200 km) with 47 vertical layers in the atmosphere. They were forced by observed sea surface

153 temperature (SST) and sea ice from the AMIP2 (Atmospheric Model Intercomparison Project

154 2) dataset for 1970-2009 (Taylor et al., 2000). 1970-1988 are regarded as spin-up phase so

155 that only the period 1989-2009 is considered for the analyses. The two simulations are:

156 • ECH6-REF: Simulation with the standard version of JSBACH 3.0 with a fixed

157 vegetation distribution and using a separate upper layer reservoir for bare soil

158 evaporation as described in Hagemann and Stacke (2015). Note that the latter is

159 switched off by default in JSBACH 3.0 to achieve a better performance of simulated

160 primary productivity, which is not of interest in the present study.

161 • ECH6-PF: As ECH6-REF, but using JSBACH-PF.

162 Note that both simulations used initial values of soil moisture, soil temperature and snowpack

163 that were obtained from an offline-simulation (land only) using JSBACH (as in ECH6-REF)

164 forced with WFDEI data (Weedon et al., 2014).

165 **2.3 Calculation of internal model climate variability**

166 The internal climate variability of ECHAM6/JSBACH with respect to 20-year mean values

167 has been estimated from results of three 20-year, 5-member ensembles, in which the

168 ensembles used different land-atmosphere coupling setups (deVrese et al., 2016). Within each

169 ensemble, the model setup is identical but the simulations were started using slightly differing

170 initial conditions. Following the approach of Hagemann et al. (2009), we first calculated the

171 standard deviation of 20-year means for each ensemble, and then the spread for each model

172 grid box is defined as the maximum of the three ensemble standard deviations. This spread is

173 then used as an estimate of the model's internal climate variability. Thus, if simulated

174 differences between ECH6-PF and ECH6-REF are larger than this spread, they are considered

175 as robust and directly related to the introduction of cold region soil processes into JSBACH.

Earth System
Dynamics
Discussions

2.4 Observational data

We use climatological observed river discharges from the station network of the Global

Runoff Data Centre (Dümenil Gates et al., 2000). Near surface air (2m) temperature and

precipitation are taken from the global WATCH dataset of hydrological forcing data (WFD;

Weedon et al., 2014). The WFDEI combine the daily statistics of the Interim re-analysis of

the European Centre for Medium-Range Weather Forecasts (ERA-Interim; Dee et al., 2011)

with the monthly mean observed characteristics of temperature from the Climate Research

Unit dataset TS2.1 (CRU; Mitchell and Jones, 2005) and precipitation from the Global

Precipitation Climatology Centre full dataset version 4 (GPCC; Fuchs et al., 2007). For the

latter, a gauge-undercatch correction following Adam and Lettenmaier (2003) was used,

which takes into account the systematic underestimation of precipitation measurements that

have an error of up to 10-50% (see, e.g. Rudolf and Rubel, 2005).

For an estimate of observed evapotranspiration (ET), we are using data from the LandFlux-

EVAL dataset. This new product was generated to compile multi-year global merged

benchmark synthesis products based on the analyses of existing land evapotranspiration

datasets (monthly time scale, time periods 1989-1995 and 1989-2005). The calculation and

analyses of the products are described in Mueller et al. (2013). In our study we are using the

diagnostic products available for the period 1989-2005 that are based on various observations,

i.e. from remote sensing, diagnostic estimates (atmospheric water-balance estimates) and

ground observations (flux measurements). Here, we considered the mean, minimum and

maximum of the respective diagnostic ensemble.

Surface solar irradiance (SSI; 2000-2010) is taken from the Clouds and Earth Radiation

Energy System (CERES; Kato et al., 2013) that provides surface solar radiation fluxes at

global scale derived from measurements onboard of the EOS Terra and Aqua satellites (Loeb

200   et al., 2012). We used surface albedo data from MODIS (MCD43C3, ver5; 2000-2011;

201   Cescatti et al., 2012), CERES (2000-2010) and the GlobAlbedo project (1998-2011; Muller et

202   al., 2012) of the European Space Agency (ESA). With regard to the accumulated snowpack,

203   we compared model data to snow water equivalent data from the ESA GlobSnow project

204   (Takala et al., 2011), NASA's Modern-Era Retrospective Analysis for Research and

205   Applications (MERRA; 1979-2013; Rienecker et al., 2011) and the snow data climatology

206   (SDC) of Foster and Davy (1988).

207   ### 2.5 Permafrost extent

208   Observational datasets of permafrost extent usually give three or four classes of spatial

209   permafrost occurrence, where the respective percentage of permafrost covered area is > 90 %

210   ('continuous'), between 90 and 50 % ('discontinuous'), < 50 % ('sporadic'), and, in some

211   references, < 10 % ('isolated'). This is the case in the data of Brown et al. (1997) shown here

212   in Fig. 1a. In most climate models, such a diversification of permafrost classes is not possible.

213   In those models as well as in JSBACH, soil temperatures are computed for one point at the

214   centre of a grid cell, thereby representing the whole area of that cell. Consequently, no 'non-

215   continuous' permafrost can be computed by JSBACH. Thus, the comparison of simulated with

216   observed permafrost extents focuses on the continuous class in the observations.

217   In order to diagnose permafrost extent from JSBACH output, its fifth layer soil temperature

218   has been extracted and checked whether it has been lower than 0 °C for more than two years

219   in a row. This criterion was applied to a 30 year time series of monthly means (1979-2009),

220   and during every proceeding month, the sum of 'permafrost months' have been set into

221   relationship to the total number of months in the time series analysed so far. This enables us

222   to have temporal variation, and avoid 'loosing' permafrost areas where it simply did not occur

223   during the last two years of the analysed time series.

3 Results

224

225 Initially, the simulated permafrost extents are compared with the data of Brown et al. (1997)

226 in Fig. 1. The implementation of permafrost relevant soil processes into JSBACH leads to an

227 improved permafrost representation in terms of continuous permafrost extent, as the too large

228 extent in western Siberia as well as in Alaska decreases in ECH-PF. Reasons for this

229 improvement are presumably the changed snow scheme and the separation of snow and soil

230 temperatures on the one hand, and the new formulation of the soil thermal properties on the

231 other hand. Combined with the organic top layer, they change the conditions for heat transfer

232 into and within the ground, which leads to more realistic deep soil temperatures in the above

233 mentioned regions.

234 Then, both simulations are evaluated over the northern high latitudes analogously to the

235 evaluation of surface water and energy fluxes of the CMIP5 version of MPI-ESM by

236 Hagemann et al. (2013b). The main differences in precipitation and 2m temperature between

237 both simulations occur in the boreal summer. In ECH6-PF, precipitation is generally reduced

238 compared to ECH-REF over the northern high latitudes (Fig. 2). On the one hand, this leads

239 to a general reduction of the wet bias compared to WFDEI data over the more continental

240 areas north of about 60°N, especially over Canada and Russia. On the other hand, it enhances

241 the dry bias over the adjacent mid-latitudes. Note that this summer dry bias of MPI-ESM 1.1

242 over mid-latitudes is more pronounced and wide-spread than in the CMIP5 version of MPI-

243 ESM (cf. Fig. 4, middle row, in Hagemann et al., 2013b), which is likely associated with bug-

244 fixes or the re-calibration of cloud processes in ECHAM6.3 (cf. Sect. 2.1). The same is also

245 the case for northern hemisphere summer warm biases in ECH6-REF (Fig. 3). These warm

246 biases are enhanced in ECH6-PF. This enhancement is partly related to the fact that the

247 reduced precipitation is accompanied by a reduced cloud cover, and, hence an increased

248   incoming solar radiation at the land surface (Fig. 4). Compared to CERES data, the low bias

249   in SSI over the high latitudes is largely removed while the overestimation over the mid-

250   latitudes is slightly increased. The reason for the warmer air temperatures can partly be found

251   in a decreased evapotranspiration (ET) when permafrost relevant physical soil processes are

252   switched on. A detailed analysis of their effects was carried out to elucidate the specific

253   influence of these processes and is shown for two large example catchments (Fig. 5). 1) The

254   Arctic catchment is represented by the six largest rivers flowing into the Arctic Ocean:

255   Kolyma, Lena, Mackenzie, Northern Dvina, Ob and Yenisei. The associated catchments

256   comprise a large fraction of permafrost covered areas (cf. Fig. 1). 2) The Baltic Sea catchment

257   includes only a low amount of permafrost covered areas but soil moisture freezing still plays a

258   role over large parts of the catchment during the winter.

259   *Arctic River catchments*

260   ECH6-PF simulates the discharge of the six largest Arctic rivers more reliably than ECH6-

261   REF, especially with regard to timing and size of the snow melt induced discharge peak in

262   spring (Fig. 6a). This is largely related to the fact that in ECH6-PF, a major part of the snow

263   melt turns into surface runoff as it cannot infiltrate into the ground when this is still frozen in

264   the beginning of spring. This is opposite to ECH6-REF where larger parts of the snow melt

265   are infiltrating into the soil due to the missing freezing processes such that the observed

266   discharge peak is largely underestimated.

267   Also with regard to precipitation, ECH6-PF shows a large improvement in the simulated

268   summer precipitation as the large wet bias of ECH6-REF is strongly reduced and, hence,

269   much closer to WFDEI data (Fig. 6c). This reduction in summer precipitation is accompanied

270   by a reduction in summer evapotranspiration (Fig. 7a) that is now much closer to the mean of

271   diagnostic estimates from the LandFlux dataset, while it is likely overestimated in ECH6-REF

272   as the simulated evapotranspiration is close to the upper limit of the LandFlux diagnostic

273   estimates. This ET reduction in ECH6-PF is directly related to a completely changed seasonal

274   cycle of liquid relative soil moisture (actual soil moisture divided by the maximum soil water

275   holding capacity) in the root zone (Fig. 7c). In ECH6-REF, the soil is very wet throughout the

276   whole year with somewhat lower values in summer that are related to the summer ET. In

277   ECH6-PF, the soil is rather dry in winter as larger parts of the soil moisture are frozen (Fig.

278   8), and, hence, not accessible for ET. With infiltration of snowmelt in the spring when the soil

279   water of the upper layer has melted, the soil moisture is increasing and reaches its maximum

280   in summer. The total amount of liquid soil moisture in ECH6-PF is much lower than in

281   ECH6-REF. On the one hand large parts of the soil are frozen in winter and adjacent months

282   (Fig. 8), and on the other hand this is related to the much lower infiltration in spring, so that

283   less moisture is available throughout the whole year. In the autumn and winter, the total

284   amount of soil water is somewhat increasing (Fig. 7c) as due to freezing, it is locally bound

285   and can neither flow off laterally nor evaporate. If compared to the model's internal climate

286   variability (Fig. 9) we note that the differences between ECH6-PF and ECH6-REF are robust

287   for ET and precipitation from April-October and April-August, respectively.

288   The decreased ET during warm months, however, brings about less evaporative cooling of the

289   land surface, and near surface air temperature increases with the use of the PF scheme. This

290   results in a further increase of the warm bias in 2m air temperature in comparison to WFDEI

291   data (Fig. 10a). Parts of the summer warm bias is caused by an overestimated incoming

292   surface solar irradiance (SSI). In ECH6-REF, the simulated SSI is close to CERES data (Fig.

293   10c), but in ECH6-PF the reduced ET leads to a reduced upward moisture flux into the

294   atmosphere that in turn seems to reduce cloud cover, and, hence SSI is increased.

295   The surface albedo is rather similar in both experiments (Fig. 11a) but shows some distinct

Earth System
Dynamics
Discussions

296 biases if compared to various observational datasets. During the winter JSBACH seems to

297 overestimate the mainly snow-related albedo, indicating that it may have difficulties to

298 adequately represent snow-masking effect of boreal forests (Note that a version of MODIS

299 albedo data was used where low quality data over the very high northern latitudes were

300 filtered out in the boreal winter due to too low available radiation (A. Löw, pers. comm.,

301 2016). Due to these missing data over mainly snow covered areas, MODIS albedo averaged

302 over the six largest Arctic rivers is biased low in the winter). During the summer, there is a

303 larger uncertainty in the observations. While the simulated albedo is close to MODIS and

304 CERES data, it is lower than GlobAlbedo data. As a too low albedo would lead to a warm

305 bias, this might indicate a better reliability of the GlobAlbedo data for this region in summer.

306 Note that a sensitivity test where surface albedo was increased by 0.05 north of 60°N led to a

307 reduction of the warm bias by about 1-2 K (not shown). As already indicated by the surface

308 albedo, the simulated snow cover does not significantly differ between the experiments, either

309 (Fig. 11c). It is lower than various observational estimates, which should impose a low albedo

310 bias in winter. As this bias is in the opposite direction, it can be concluded that the low snow

311 pack is compensating part of the snow masking problem mentioned above.

312 *Baltic Sea catchment*

313 A similar effect of the frozen ground is found over the Baltic Sea catchment, although this is

314 less strong than for the Arctic rivers. The frozen ground leads to an enhanced snow melt

315 runoff in spring (Fig. 6b) and a less strong replenishment of the ground by water during the

316 winter as it is the case for ECH6-REF (Fig. 7d). Consequently the average level of liquid soil

317 moisture is lower in ECH6-PF compared to ECH6-REF. This leads to more infiltration of

318 water and less drainage, and hence, less runoff in the summer, which in turns leads to an

319 improved simulation of discharge (Fig. 6b). The impact on the atmosphere is much less

Earth System
Dynamics
Discussions

EGU

Open Access

320   pronounced than for the Arctic rivers. On one hand there is less frozen ground in the Baltic

321   Sea catchment (Fig. 8), on the other hand the average soil moisture content is larger than for

322   the Arctic rivers (Fig. 7d). In ECH6-REF, the soil moisture is generally above W_{crit} (c.f. Sect.

323   1) over the Baltic Sea catchment so that ET is largely energy limited and mostly occurring at

324   its potential rate. Even though the ECH6-PF soil moisture is lower, it is generally still close to

325   W_{crit} so that ET is only slightly reduced, especially in the second half of the year (Fig. 7b).

326   Precipitation is also somewhat reduced (Fig. 6d) but this seems to be mostly related to the

327   internal climate variability except for September and October when a somewhat stronger and

328   robust reduction in ET leads to a robust precipitation decrease (Fig. 9).

329   **4   Discussion and conclusions**

330   The results described in the previous section show that the introduction of cold region

331   processes into MPI-ESM led to a positive soil moisture-precipitation feedback over large

332   parts of northern mid- and high latitudes during the boreal summer. The chain of processes

333   leading to this feedback is sketched in Fig. 12. The frozen soil during the cold season (late

334   autumn to early spring) leads to less infiltration of rainfall and snowmelt during this season,

335   and, hence, to more surface runoff especially during the snowmelt period. On one hand this

336   leads to a large improvement in simulated discharge, mainly due to the improved snowmelt

337   peak. This improved discharge due to the representation of frozen ground has been also

338   reported for other models (Beer et al., 2006, 2007; Ekici et al., 2014; Gouttevin et al., 2012).

339   On the other hand, this leads to a decrease of soil moisture. During the boreal summer, this

340   actually causes more infiltration and less runoff, and, hence, less discharge. The latter strongly

341   improves the simulated discharge in the Baltic Sea catchment from summer to early winter.

342   The decreased soil moisture leads to a reduced ET in regions where the soil moisture is in the

343   transitional regime. Here, there is less recycling of moisture into the atmosphere, and the

344   lower atmospheric moisture causes a reduction of precipitation that in turn leads to a further

345   reduction of soil moisture. This positive soil moisture-precipitation feedback improves the

346   simulated hydrological cycle, especially over the Arctic rivers where the wet biases in

347   summer precipitation and ET are reduced. Less ET, and, hence, less evaporative cooling cause

348   an increase in summer 2m air temperatures. This, in combination with more incoming surface

349   solar radiation due to fewer clouds, increases and extends the existing summer warm bias of

350   MPI-ESM north of about 50°N.

351   Such a positive soil moisture-precipitation feedback has not been pointed out for the northern

352   high latitudes so far, which previously have generally been considered as energy-limited

353   regimes where land-atmosphere coupling due to soil moisture does not play a role (e.g.

354   Teuling et al., 2009). But this principal feedback loop has been found for drier regions where

355   the soil moisture is generally in the transitional regime and land-atmosphere coupling plays a

356   role. Koster et al. (2004) considered the strength of coupling between soil moisture and

357   precipitation in an ensemble of atmospheric GCMs. The resulting map is very similar to the

358   map regarding the strength of coupling between soil moisture and temperature in the same

359   GCMs (Koster et al., 2006). This suggests that in these models, the same process controls

360   both couplings, namely the ET sensitivity to soil moisture that leads to a positive feedback

361   (Seneviratne et al., 2010). But in those studies (Koster et al., 2004; Teuling et al., 2009),

362   usually annual mean diagnostics were considered. Our study has shown that seasonally, i.e.

363   during the boreal summer, soil moisture conditions may prevail that allow for land-

364   atmosphere coupling and a positive soil moisture-precipitation feedback over the northern

365   high and mid-latitudes.

366   Even though our results are obtained with a modelling study, their physical consistency

367   suggests that cold region soil processes, especially melting and freezing of soil moisture, may

Earth System Dynamics

Discussions

Open Access

EGU

368   lead to a positive soil moisture precipitation feedback during the summer in reality, too. A

369   prerequisite for the occurrence of a soil moisture precipitation feedback is that soil moisture is

370   in the transitional regime. Thus, the strength of the feedback depends on the wetness of the

371   soil and, hence, is likely model dependent. Models with wetter/drier soils over the considered

372   regions may simulate a weaker/stronger feedback.

373   Several modelling studies pointed out that there are not only positive feedback loops between

374   soil moisture and precipitation but also negative ones that, under specific conditions, such as

375   convective instability and/or cloud formation, may be stronger over dry soils (e.g.

376   Hohenegger et al., 2009; Froidevaux et al., 2014). However, to date, the latter results appear

377   mostly confined to single-column, cloud-resolving, and some high-resolution regional climate

378   simulations (Seneviratne et al., 2010) and may also depend on the choice of the convective

379   parameterisations (e.g. Giorgi et al., 1996). Guillod et al. (2015) noted that precipitation

380   events tend to be located over drier patches, but they generally need to be surrounded by wet

381   conditions; positive temporal soil moisture-precipitation relationships are thus driven by

382   large-scale soil moisture. Thus, negative feedbacks seem to have more an impact on high

383   resolution and thus on the local scale (Ho-Hagemann et al., 2015), where the effects of land

384   surface heterogeneity for the inferred feedbacks also need to be taken into account (Chen and

385   Avissar, 1994; Pielke et al., 1998; Taylor et al., 2013). Consequently most GCMs may not be

386   able to represent negative feedbacks between soil moisture and precipitation via ET. As in the

387   present study, we considered the effect of large-scale soil moisture changes due to soil

388   freezing processes, the identification of potential negative feedbacks on the local scale is not

389   an issue.

390   In MPI-ESM, an unwelcome effect of implementing cold region soil processes is the increase

391   of the existing warm bias over the high latitudes during summer. In order to estimate the

392   contribution of biases in SSI and surface albedo to this warm bias, we calculated an upper

393   limit for the temperature change that may be imposed by a radiation difference in the related

394   energy flux into the ground [SSI × (1 – albedo)]. For this estimation we assume that the

395   surface temperature is adjusting in a way that this radiation difference is compensated by

396   thermal radiation following the Stefan Boltzmann law. Here, any change in the turbulent

397   surface heat fluxes is neglected so that the resulting temperature change is an upper limit for

398   the temperature bias that might be explained by a radiation bias.

399   Considering the mean summer biases over the six largest Arctic rivers (Table 1) indicates that

400   a part of the warm bias may be attributed to the overestimation in SSI. For ECH6-PF (ECH6-

401   REF), the SSI bias may cause a warm bias of up to 2.9 K (0.9 K). The surface albedo may

402   contribute another 0.7 K (0.8 K) to the warm bias if compared to GlobAlbedo data but this is

403   a rather vague estimation due to the large uncertainty on surface albedo observations (see Fig.

404   11). Nevertheless biases in both of these variables cannot explain the full bias of 5 K (2.1 K)

405   in 2m temperature. Further contributions to this warm bias might be related to too much

406   advection of warm air or a too weak vertical mixing of heat within the boundary layer. A

407   deeper investigation of this is beyond the scope of the present study and should be dealt with

408   in future model improvements.

409   We have shown that biophysical land surface processes such as melting and freezing can have

410   a significant impact on the regional climate over the high latitudes and permafrost areas. Flato

411   et al. (2013) reported that CMIP5 GCMs tend to overestimate precipitation over northern high

412   latitudes except for Europe and western Siberia. As many of these GCMs are still missing

413   basic cold region processes (see Sect. 1), a missing soil moisture precipitation feedback in

414   those GCMs might contribute to this wet bias. Beyond the biophysical coupling between land

415   and atmosphere, the coupling to biogeochemistry, i.e. vegetation and carbon cycle including

Earth System Dynamics
Discussions

416   methane and frozen carbon, is important to quantify feedbacks related to wetlands and

417   permafrost over those areas. The representation of their complex dynamics within ESMs is a

418   challenging task, but it is nevertheless necessary to investigate on-going and future climate

419   changes over the high-latitude regions. Thus, the adequate implementation of physical soil

420   processes into an ESM is only the first necessary step to yield an adequate representation of

421   climate feedbacks over the high latitudes. This also includes the incorporation of wetland

422   dynamics, which will be the next step in the JSBACH development with regard to high

423   latitudes, thereby following an approach of Stacke and Hagemann (2012).

424   **Acknowledgments**

428   **References**

429   ACIA: Arctic Climate Impact Assessment, Cambridge University Press, 1042p.,

430   http://www.acia.uaf.edu, 2005.

431   Adam, J. C., and, Lettenmaier, D. P.: Adjustment of global gridded precipitation for

432   systematic bias, J. Geophys. Res., 108, D9, 4257, doi:10.1029/2002JD002499, 2003.

433   Beer, C., Lucht, W., Schmullius, C., and Shvidenko, A.: Small net carbon dioxide uptake by

434   Russian   forests   during   1981–1999,   Geophys.   Res.   Lett.,   33,   L15403,

435   doi:10.1029/2006GL026919, 2006.

436   Beer, C., Lucht, W., Gerten, D., Thonicke, K., and Schmullius, C.: Effects of soil freezing and

437   thawing on vegetation carbon density in Siberia: A modeling analysis with the Lund-

438   Potsdam-Jena Dynamic Global Vegetation Model (LPJ-DGVM), Global Biogeochem.

Earth System
Dynamics
Discussions

439   Cyc., 21, GB1012, doi:10.1029/2006GB002760, 2007.

440   Brovkin, V., Raddatz, T., Reick, C. H., Claussen, M., and Gayler, V.: Global biogeophysical

441   interactions between forest and climate, Geophys. Res. Letters, 36, L07 405,

442   doi:10.1029/2009GL037543, 2009.

443   Brown, J., Ferrians Jr., O. J., Heginbottom, J. A., and Melnikov, E. S. (eds.): Circum-Arctic

444   map of permafrost and ground-ice conditions, Washington, DC: U.S. Geological Survey

445   in Cooperation with the Circum-Pacific Council for Energy and Mineral Resources.

446   Circum-Pacific Map Series CP-45, scale 1:10,000,000, 1997.

447   Cescatti, A., Marcolla, B., Santhana Vannan, S. K., Pan, J. Y., Román, M. O., Yang, X.,

448   Ciais, P., Cook, R. B., Law, B. E., Matteucci, G., Migliavacca, M., Moors, E.,

449   Richardson, A. D., Seufert, G., and Schaaf, C.B.: Intercomparison of MODIS albedo

450   retrievals and in situ measurements across the global FLUXNET network, Rem. Sens.

451   Environ., 121, 323-334, 2012.

452   Chen, F., and Avissar, R.: Impact of land-surface moisture variability on local shallow

453   convective cumulus and precipitation in large-scale models, J. Appl. Meteorol., 33 (12),

454   1382–1401, 1994.

455   Cox, P., Betts, R., Bunton, C., Essery, R., Rowntree, P., and Smith, J.: The impact of new

456   land surface physics on the GCM simulation. of climate and climate sensitivity, Climate

457   Dyn., 15, 183–203, doi:10.1007/s003820050276, 1999.

458   de Vrese, P., and Hagemann, S.: Explicit representation of spatial sub-grid scale heterogeneity

459   in an ESM, J. Hydrometeorol., submitted, 2016.

460   Dee, D. P., Uppala, S. M., Simmons, A. J., Berrisford, P., Poli, P., Kobayashi, S., Andrae, U.,

461   Balmaseda, M. A., Balsamo, G., Bauer, P., Bechtold, P., Beljaars, A. C. M., van de Berg,

462   L., Bidlot, J., Bormann, N., Delsol, C., Dragani, R., Fuentes, M., Geer, A. J., Haimberger,

Earth System
Dynamics
Discussions

463   L., Healy, S. B., Hersbach, H., Hólm, E. V., Isaksen, L., Kållberg, P., Köhler, M.,

464   Matricardi, M., McNally, A. P., Monge-Sanz, B. M., Morcrette, J.-J., Park, B.-K.,

465   Peubey, C., de Rosnay, P., Tavolato, C., Th´epaut, J.-N., and Vitart, F.: The ERA-interim

466   reanalysis: configuration and performance of the data assimilation system, Q. J. Roy.

467   Meteorol. Soc., 137, 553–597, doi:10.1002/qj.828, 2011.

468 Dirmeyer, P., Koster, R., and Guo, Z. A. D.: Do global models properly represent the

469   feedback between land and atmosphere?, J. Hydrometeorol., 7, 1177–1198, 2006.

470 Dümenil Gates, L., Hagemann, S., and Golz, C.: Observed historical discharge data from

471   major rivers for climate model validation, Max Planck Institute for Meteor. Rep., 307

472   [available from MPI for Meteorology, Bundesstr. 53, 20146 Hamburg, Germany], 2000.

473 Ekici, A., Beer, C., Hagemann, S., Boike, J., Langer, M., and Hauck, C.: Simulating high

474   latitude permafrost regions by the JSBACH terrestrial ecosystem model, Geosci. Model

475   Dev., 7, 631-647, doi:10.5194/gmd-7-631-2014, 2014.

476 Ekici, A., Chadburn, S., Chaudhary, N., Hajdu, L. H., Marmy, A., Peng, S., Boike, J., Burke,

477   E., Friend, A. D., Hauck, C., Krinner, G., Langer, M., Miller, P. A., and Beer, C.: Site-

478   level model intercomparison of high latitude and high altitude soil thermal dynamics in

479   tundra and barren landscapes, The Cryosphere, 9, 1343-1361, doi:10.5194/tc-9-1343-

480   2015, 2015.

481 Flato, G., Marotzke, J., Abiodun, B., Braconnot, P., Chou, S. C., Collins, W., Cox, P.,

482   Driouech, F., Emori, S., Eyring, V., Forest, C., Gleckler, P., Guilyardi, E., Jakob, C.,

483   Kattsov, V., Reason, C., and Rummukainen, M.: Evaluation of Climate Models. In:

484   Climate Change 2013: The Physical Science Basis, Contribution of Working Group I to

485   the Fifth Assessment Report of the Intergovernmental Panel on Climate Change [Stocker,

486   T.F., Qin, D., Plattner, G.-K., Tignor, M., Allen, S. K., Boschung, J., Nauels, A., Xia, Y.,

Earth System
Dynamics

Discussions

487   Bex, V., and Midgley, P. M. (eds.)]. Cambridge University Press, Cambridge, United

488   Kingdom and New York, NY, USA, 2013.

489   Foster, D. J., and Davy, R.D.: Global snow data climatology, USAFETAC/TN-88/006, Scott

490   Air Force Base III, 1988.

491   French, H. M.: Editorial, Permafrost Periglac. Process, 1, 1, doi: 10.1002/ppp.3430010102,

492   1990.

493   Froidevaux, P., Schlemmer, L., Schmidli, J., Langhans, W., and Schär, C.: Influence of

494   background wind on the local soil moisture-precipitation feedback, J. Atmos. Sci., 71,

495   782-799, 2014.

496   Fuchs, T., Schneider, U., and Rudolf, B.: Global Precipitation Analysis Products of the

497   GPCC, Global Precipitation Climatology Centre (GPCC). Deutscher Wetterdienst,

498   Offenbach, Germany, 2007.

499   Giorgi, F., Mearns, L.O., Shields, C., and Mayer, L.: A regional model study of the

500   importance of local versus remote controls of the 1988 drought and the 1993 flood over

501   the central United States, J. Climate, 9, 1150–1162, 1996.

502   Goll, D. S., Brovkin, V., Liski, J., Raddatz, T., Thum, T., and Todd-Brown, K. E. O.: Strong

503   dependence of CO2 emissions from anthropogenic land cover change on initial land cover

504   and soil carbon parametrization, Global Biogeochem. Cycles, 29, 1511–1523,

505   doi:10.1002/2014GB004988, 2015.

506   Gouttevin, I., Krinner, G., Ciais, P., Polcher, J., and Legout, C.: Multi-scale validation of a

507   new soil freezing scheme for a land-surface model with physically-based hydrology, The

508   Cryosphere, 6, 407-430, doi:10.5194/tc-6-407-2012, 2012.

509   Guillod, B. P., Orlowsky, B., Miralles, D. G., Teuling, A. J., and Seneviratne, S. I.:

510   Reconciling spatial and temporal soil moisture effects on afternoon rainfall, Nat.

511   Commun., 6, 6443, doi: 10.1038/ncomms7443, 2015.

512   Hagemann, S., Göttel, H., Jacob, D., Lorenz, P., and Roeckner, E.: Improved regional scale

513   processes reflected in projected hydrological changes over large European catchments,

514   Climate Dyn., 32, 767-781, doi: 10.1007/s00382-008-0403-9, 2009.

515   Hagemann, S., Blome, T., Saeed, F., and Stacke, T.: Perspectives in modelling climate-

516   hydrology interactions, Surveys in Geophys., 35, 739-764, ISSI special issue on

517   Hydrological Cycle, doi:10.1007/s10712-013-9245-z, 2013a.

518   Hagemann, S., Loew, A., Andersson, A.: Combined evaluation of MPI-ESM land surface

519   water and energy fluxes, J. Adv. Model. Earth Syst., 5, doi:10.1029/2012MS000173,

520   2013.

521   Hagemann, S., and Stacke, T.: Impact of the soil hydrology scheme on simulated soil

522   moisture memory, Climate Dyn., 44, 1731-1750, doi:10.1007/s00382-014-2221-6, 2015.

523   Ho-Hagemann, H. T. M., Rockel, B., and Hagemann, S.: On the role of soil moisture in the

524   generation of heavy rainfall during the Oder flood event in July 1997, Tellus A, 67,

525   28661, dx.doi.org/10.3402/tellusa.v67.28661, 2015.

526   Hohenegger, C., Brockhaus, P., Bretherton, C. S., and Schär, C.: The Soil Moisture–

527   Precipitation Feedback in Simulations with Explicit and Parameterized Convection, J.

528   Climate, 22, 5003–5020, 2009.

529   Kato, S., Loeb, N. G., Rose, F. G., Doelling, D. R., Rutan, D. A., Caldwell, T. E., Yu, L., and

530   Weller, R. A.: Surface irradiances consistent with CERES-derived top-of-atmosphere

531   shortwave and longwave irradiances, J. Climate, 26, 2719-2740, doi: 10.1175/JCLI-D-12-

532   00436.1, 2013.

533   Koren, V., Schaake, J., Mitchell, K., Duan, O. Y., Chen, F., and Baker, J. M.: A

534   parameterization of snowpack and frozen ground intended for NCEP weather and climate

Earth System
Dynamics
Discussions

EGU

535   models, J. Geophys. Res., 104, 19569–19585, 1999.

536   Koster, R. D., Dirmeyer, P. A., Guo, Z., Bonan, G., Chan, E., Cox, P., Gordon, C. T., Kanae,

537   S., Kowalczyk, E., Lawrence, D., Liu, P., Lu, C. H., Malyshev, S., McAvaney, B.,

538   Mitchell, K., Mocko, D., Oki, T., Oleson, K., Pitman, A., Sud, Y. C., Taylor, C. M.,

539   Verseghy, D., Vasic, R., Xue, Y., and Yamada, T.: Regions of strong coupling between

540   soil moisture and precipitation, Science, 305, 1138–1140, 2004.

541   Koster R. D., Guo, Z., Dirmeyer, P. A., Bonan,, G., Chan, E., Cox, P., Davies, H., Gordon, C.

542   T., Kanae, S., Kowalczyk, E., Lawrence, D., Liu, P., Lu, C. H., Malyshev, S., McAvaney,

543   B., Mitchell, K., Mocko, D., Oki, T., Oleson, K. W., Pitman, A., Sud, Y. C., Taylor, C.

544   M., Verseghy, D., Vasic, R., Xue, Y., and Yamada, T.: GLACE: The Global Land-

545   Atmosphere Coupling Experiment. Part I: Overview, J. Hydrometeorol., 7, 590–610,

546   2006.

547   Koven, C. D., Riley, W. J., and Stern, A.: Analysis of permafrost thermal dynamics and

548   response to climate change in the CMIP5 Earth System Models, J. Climate, 26, 1877-

549   1900, doi:10.1175/JCLI-D-12-00228.1, 2012.

550   Lawrence, D. M., and Slater, A. G.: A projection of severe near-surface permafrost

551   degradation during the 21st century, Geophys. Res. Lett., 32, L24401,

552   doi:10.1029/2005GL025080, 2005.

553   Loeb, N. G., Kato, S., Su, W., Wong, T., Rose, F. G., Doelling, D. R., and Norris, J.:

554   Advances in understanding top-of-atmosphere radiation variability from satellite

555   observations, Surveys in Geophysics, doi: 10.1007/s10712-012-9175-1, 2012.

556   Luo, L. F., Robock, A., Vinnikov, K. Y., Schlosser, C. A., Slater, A. G., Boone, A., Braden,

557   H., Cox, P., de Rosnay, P., Dickinson, R. E., Dai, Y. J., Duan, Q. Y., Etchevers, P.,

558   Henderson-Sellers, A., Gedney, N., Gusev, Y. M., Habets, F., Kim, J. W., Kowalczyk, E.,

559   Mitchell, K., Nasonova, O. N., Noilhan, J., Pitman, A. J., Schaake, J., Shmakin, A. B.,

560   Smirnova, T. G., Wetzel, P., Xue, Y. K., Yang, Z. L., and Zeng, Q. C.: Effects of frozen

561   soil on soil temperature, spring infiltration, and runoff: Results from the PILPS 2(d)

562   experiment at Valdai, Russia, J. Hydrometeorol., 4, 334–351, 2003.

563   McGuire, A. D., Anderson, L. G., Christensen, T. R., Dallimore, S., Guo, L., Hayes, D. J.,

564   Heimann, M., Lorenson, T. D., Macdonald, R. W., and Roulet, N.: Sensitivity of the

565   carbon cycle in the Arctic to climate change, Ecological Monographs, 79, 523–555,

566   doi:10.1890/08-2025.1, 2009.

567   Meehl, G. A., Boer, G. J., Covey, C., Latif, M., and Stouffer, R. J.: The Coupled Model

568   Intercomparison Project (CMIP), Bull. Amer. Meteor. Soc., 81, 313–318, 2000.

569   Mitchell, T. D., and Jones, P. D.: An improved method of constructing a database of monthly

570   climate observations and associated high-resolution grids, Int. J. Climatol., 25, 693-712,

571   2005.

572   Mueller, B., Hirschi, M., Jimenez, C., Ciais, P., Dirmeyer, P. A., Dolman, A. J., Fisher, J. B.,

573   Jung, M., Ludwig, F., Maignan, F., Miralles, D., McCabe, M. F., Reichstein, M.,

574   Sheffield, J., Wang, K. C., Wood, E. F., Zhang, Y., and Seneviratne, S. I.: Benchmark

575   products for land evapotranspiration: LandFlux-EVAL multi-dataset synthesis, Hydrol.

576   Earth Syst. Sci., 17, 3707-3720, doi:10.5194/hess-17-3707-2013, 2013.

577   Muller, J.-P., López, G., Watson, G., Shane, N., Kennedy, T., Yuen, P., Lewis, P., Fischer, J.,

578   Guanter, L., Domench, C., Preusker, R., North, P., Heckel, A., Danne, O., Krämer, U.,

579   Zühlke, M., Brockmann, C., and Pinnock, S.: The ESA GlobAlbedo Project for mapping

580   the Earth's land surface albedo for 15 Years from European Sensors., paper presented at

581   IEEE Geoscience and Remote Sensing Symposium (IGARSS) 2012, IEEE, Munich,

582   Germany, 22-27.7.12, 2012.

583   Pielke, R.A., Avissar, R., Raupach, M., Dolman, A.J., Zeng, X.B., and Denning, A.S.:

584   Interactions between the atmosphere and terrestrial ecosystems: influence on weather and

585   climate, Glob. Chang. Biol. 4 (5), 461–475, 1998.

586   Raddatz, T. J., Reick, C., Knorr, W., Kattge, J., Roeckner, E., Schnur, R., Schnitzler, K.-G.,

587   Wetzel, P., and Jungclaus, J. H.: Will the tropical land biosphere dominate the climate-

588   carbon cycle feedback during the twenty-first century?, Climate Dyn., doi:

589   10.1007/s00382-007-0247-8, 2007.

590   Rienecker, M. M., Suarez, M. J., Gelaro, R., Todling, R., Bacmeister, J., Liu, E., Bosilovich,

591   M. G., Schubert, S. D., Takacs, L., Kim, G.-K., Bloom, S., Chen, J., Collins, D., Conaty,

592   A., da Silva, A., Gu, W., Joiner, J., Koster, R. D., Lucchesi, R., Molod, A., Owens, T.,

593   Pawson, S., Pegion, P., Redder, C. R., Reichle, R., Robertson, F. R., Ruddick, A. G.,

594   Sienkiewicz, M., and Woollen, J: MERRA - NASA's Modern-Era Retrospective Analysis

595   for Research and Applications, J. Climate, 24, 3624-3648, doi:10.1175/JCLI-D-11-

596   00015.1, 2011.

597   Rudolf, B., and Rubel, F.: Global precipitation, In: Hantel. M. (ed): Observed global climate,

598   Chap. 11. Landolt–Boernstein: numerical data and functional relationships in science and

599   technology – new series, Group 5: Geophysics, vol. 6, Springer, Berlin Heidelberg New

600   York, p 567, 2005.

601   Schuur, E. A. G., Bockheim, J., Canadell, J. G., Euskirchen, E., Field, C. B., Goryachkin, S.

602   V., Hagemann, S., Kuhry, P., Lafleur, P. M., Lee, H., Mazhitova, G., Nelson, F. E.,

603   Rinke, A., Romanovsky, V. E., Shiklomanov, N., Tarnocai, C., Venevsky, S., Vogel, J.

604   G., and Zimov, S. A.: Vulnerability of permafrost carbon to climate change: Implications

605   for the global carbon cycle, Bioscience, 58, 701-714, doi:10.1641/B580807, 2008.

606   Seneviratne, S. I., and Stöckli, R.: The role of land-atmosphere interactions for climate

Earth System
Dynamics
Discussions

EGU

607   variability in Europe, In: Climate Variability and Extremes during the Past 100 years,

608   Brönnimann et al. (eds.), Adv. Global. Change. Res., 33, Springer Verlag. (Book chapter),

609   2008.

610   Seneviratne, S. I., Lüthi, D., Litschi, M., and Schär, C.: Land-atmosphere coupling and

611   climate change in Europe, Nature, 443, 205-209, 2006.

612   Seneviratne, S. I., Corti, T., Davin, E., Hirschi, M., Jaeger, E. B., Lehner, I., Orlowsky, B.,

613   and Teuling, A. J.: Investigating soil moisture-climate interactions in a changing climate:

614   A review, Earth-Sci. Rev., 99, 125-161, doi:10.1016/j.earscirev.2010.02.004, 2010.

615   Serreze, M. C., and Barry, R. G.: Processes and impacts of Arctic amplification: A research

616   synthesis, Global Planet Change, 77, 85-96, doi:10.1016/j.gloplacha.2011.03.004, 2011.

617   Slater, A., Pitman, A., and Desborough, C.: Simulation of freeze thaw cycles in a general

618   circulation model land surface scheme, J. Geophys. Res., 103, 11303–1131, 1998.

619   Solomon, S., Qin, D., Manning, M., Marquis, M., Averyt, K., Tignor, M. M. B., Miller Jr., H.

620   L., and Chen, Z. (Eds.): Climate change 2007: The physical science basis, Cambridge

621   University Press, 996 pp., 2007.

622   Stacke, T., and Hagemann, S.: Development and validation of a global dynamical wetlands

623   extent scheme, Hydrol. Earth Syst. Sci., 16, 2915-2933, doi:10.5194/hess-16-2915-2012,

624   2012.

625   Stevens, B., Giorgetta, M., Esch, M., Mauritsen, T., Crueger, T., Rast, S., Salzmann, M.,

626   Schmidt, H., Bader, J., Block, K., Brokopf, R., Fast, I., Kinne, S., Kornblueh, L.,

627   Lohmann, U., Pincus, R., Reichler, T., and Roeckner, E.: The atmospheric component of

628   the MPI-M Earth System Model: ECHAM6, J. Adv. Model Earth Syst., 5, 146-172.

629   doi:10.1002/jame.20015, 2013.

630   Swenson, S. C., Lawrence, D. M., and Lee, H.: Improved simulation of the terrestrial

Earth System
Dynamics
Discussions

631   hydrological cycle in permafrost regions by the Community Land Model, J. Adv. in

632   Modelling Earth Systems, 4, doi:10.1029/2012MS000165, 2012.

633   Takala, M., Luojus, K., Pulliainen, J., Derksen, C., Lemmetyinen, J., Kärnä, J.-P, Koskinen,

634   J., and Bojkov, B.: Estimating northern hemisphere snow water equivalent for climate

635   research through assimilation of spaceborne radiometer data and ground-based

636   measurements, Rem. Sens. Environ., 115, doi: 10.1016/j.rse.2011.08.014, 2011.

637   Tarnocai, C., Canadell, J. G., Schuur, E. A. G., Kuhry, P., Mazhitova, G., and Zimov, S.: Soil

638   organic carbon pools in the northern circumpolar permafrost region, Global Biogeochem

639   Cycles, 23, doi:10.1029/2008GB003327, 2009.

640   Taylor, C. M., Birch, C. E., Parker, D. J., Dixon, N., Guichard, F., Nikulin, G., and Lister, G.

641   M. S.: Modeling soil moisture-precipitation feedback in the Sahel: Importance of spatial

642   scale versus convective parameterization, Geophys. Res. Lett., 40, 6213–6218,

643   doi:10.1002/2013GL058511, 2013.

644   Taylor, K. E., Williamson, D., and Zwiers, F.: The sea surface temperature and sea-ice

645   concentration boundary conditions for AMIP II simulations, PCMDI Report, 60, Program

646   for Climate Model Diagnosis and Intercomparison. Lawrence Livermore National

647   Laboratory, Livermore, California, 25 pp., 2000.

648   Taylor, K. E., Stouffer, R. J., and Meehl, G. A.: An overview of CMIP5 and the experiment

649   design, Bull. Amer. Meteor. Soc., 93 (4), 485-498, 2012.

650   Teuling, A. J., Hirschi, M., Ohmura, A., Wild, M., Reichstein, M., Ciais, P., Buchmann, N.,

651   Ammann, C., Montagnani, L., Richardson, A. D., Wohlfahrt, G., and Seneviratne, S. I.: A

652   regional perspective on trends in continental evaporation, Geophys. Res. Lett., 36,

653   L02404, doi:10.1029/2008GL036584, 2009.

654   Walsh, J. E., Anisimov, O., Hagen, J. O. M., Jakobsson, T., Oerlemans, J., Prowse, T. D.,

Earth System
Dynamics
Discussions

655   Romanovsky, V., Savelieva, N., Serreze, M., Shiklomanov, A., Shiklomanov, I.,

656   Solomon, S., Arendt, A., Atkinson, D., Demuth, M. N., Dowdeswell, J., Dyurgerov, M.,

657   Glazovsky, A., Koerner, R. M., Meier, M., Reeh, N., Sigurosson, O., Steffen, K., and

658   Truffer, M.: Cryosphere and hydrology, in: Symon C, Arris L, Heal B (eds.) Arctic

659   Climate Impact Assessment, Chap. 6: 184-242, Cambridge University Press, 2005.

660   Weedon, G. P., Balsamo, G., Bellouin, N., Gomes, S., Best, M. J., and Viterbo, P.: The

661   WFDEI meteorological forcing data set: WATCH Forcing Data methodology applied to

662   ERA-Interim reanalysis data, Water Resour. Res., 50, doi:10.1002/2014WR015638,

663   2014.

664   Zimov, S. A., Davydov, S. P., Zimova, G. M., Davydova, A. I., Schuur, E. A. G., Dutta, K.,

665   and Chapin III, F. S.: Permafrost carbon: Stock and decomposability of a globally

666   significant carbon pool, Geophys Res. Lett., 33, doi:10.1029/2006GL027484, 2006.

667

Earth System
Dynamics
Discussions

668 **Figure captions**

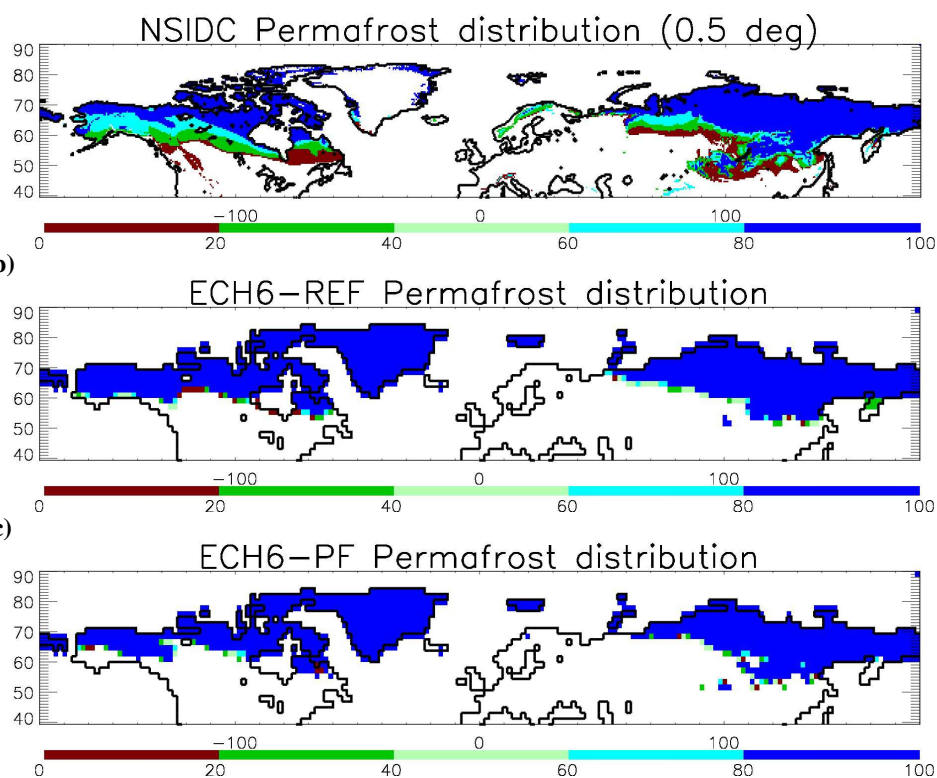669 Fig. 1 Distribution of permafrost areas in the Arctic according to a) Brown et al. (1997), b)
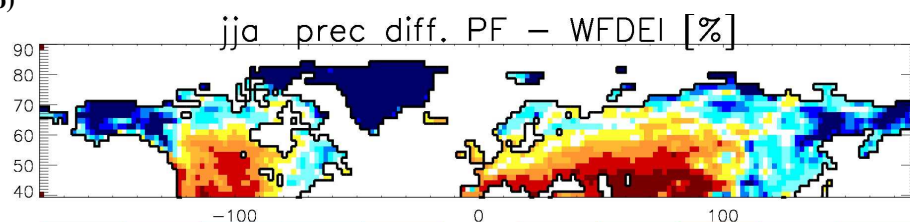
670 ECH6-REF, and c) ECH6-PF.

671 Fig. 2 Boreal summer (JJA) precipitation differences [%] relative to WFDEI data for a)

672 ECH6-REF, and b) ECH6-PF.

673 Fig. 3 Boreal summer (JJA) 2m temperature differences [K] to WFDEI data for a) ECH6-

674 REF, and b) ECH6-PF.

675 Fig. 4 Boreal summer (JJA) surface solar incoming radiation differences [W/m²] to CERES

676 data for a) ECH6-REF, and b) ECH6-PF.

677 Fig. 5 Catchments of the Baltic Sea and of the six largest Arctic rivers (from left to right:

678 Mackenzie, Baltic Sea, Northern Dvina, Ob, Yenisei, Lena, Kolyma).

679 Fig. 6 Mean monthly climatology (1989-2009) of discharge (upper panels) and

680 precipitation (lower panels) over the 6 largest Arctic river catchments (left column)

681 and the Baltic Sea catchment (land only, right column). Observations comprise

682 climatological observed discharge and WFDEI precipitation, respectively.

683 Fig. 7 Mean monthly climatology (1989-2009) of evapotranspiration (upper panels) and

684 relative root zone soil moisture (lower panels) over the 6 largest Arctic river

685 catchments (left column) and the Baltic Sea catchment (land only, right column).

686 Evapotranspiration data comprise the mean, minimum and maximum diagnostic

687 estimates from the LandFlux Eval (LF) dataset. The dashed blue line denotes the

688 total root zone water content (liquid + frozen) for ECH6-PF.

689 Fig. 8 Mean fraction of frozen root zone soil moisture (1989-2009) over the 6 largest Arctic

690 river catchments (solid curve) and the Baltic Sea catchment (land only, dashed

691 curve).

692 Fig. 9 Mean monthly climatological differences (1989-2009) of between ECH6-PF and

Earth System Dynamics

Discussions

Open Access

EGU

693   ECH6-REF for precipitation (*ΔP*) and evapotranspiration (*ΔET*) over the 6 largest

694   Arctic rivers (upper panel) and the Baltic Sea catchment (lower panel). The dashed

695   lines indicate the corresponding spreads obtained from MPI-ESM simulations of

696   deVrese et al. (2016).

697 Fig. 10 Mean monthly climatology (1989-2009) of 2m temperature differences to WFDEI

698   data (upper panels) and surface solar irradiance (SSI; lower panels) over the 6 largest

699   Arctic river catchments (left column) and the Baltic Sea catchment (land only, right

700   column). SSI observations comprise CERES data for 2000-2010.

701 Fig. 11 Mean monthly climatology (1989-2009) of surface albedo (upper panels) and snow

702   pack snow water equivalent (SWE; lower panels) over the 6 largest Arctic river

703   catchments (left column) and the Baltic Sea catchment (land only, right column).

704   Albedo observations data from MODIS (2000-2011), CERES (2000-2010) and

705   GlobAlbedo (1998-2011), SWE observations comprise data from GlobSnow (1989-

706   2009), MERRA (1979-2013), and SDC climatology.

707 Fig. 12 Chain of processes involved in the soil moisture precipitation feedback over high

708   latitudes. Red arrows indicate directions supporting this feedback, blue arrows

709   indicate compensating opposite effects.

710

711

712

Earth System
Dynamics

Open Access

EGU

Discussions

713

714
715 **b)**

716
717 **c)**

718
719
720 **Fig. 1.**   Distribution of permafrost areas in the Arctic according to a) Brown et al.
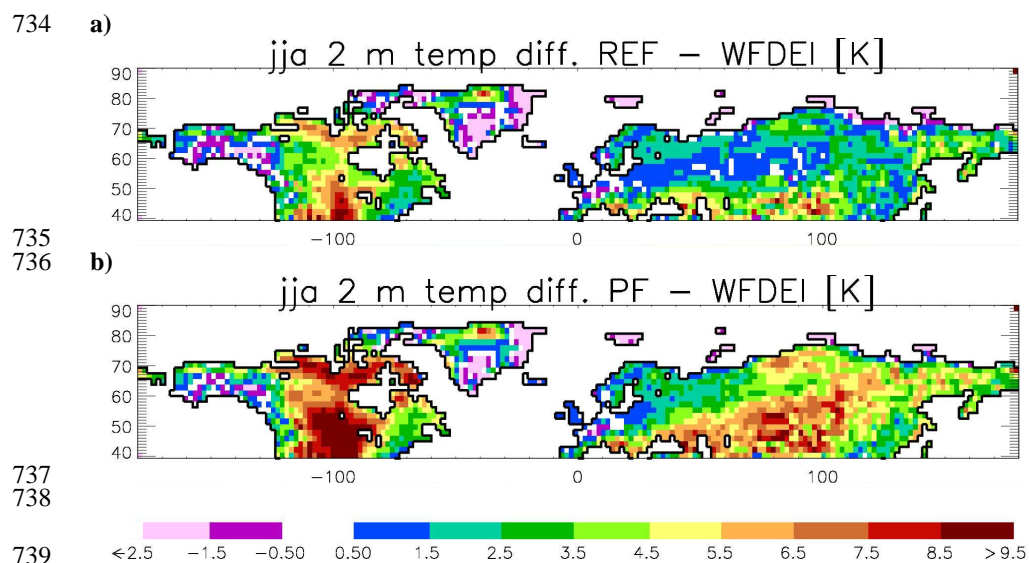721   (1997), b) ECH6-REF, and c) ECH6-PF.

722

Earth System
Dynamics
Discussions

Open Access

EGU

723   **a)**

724
725   **b)**

726
727
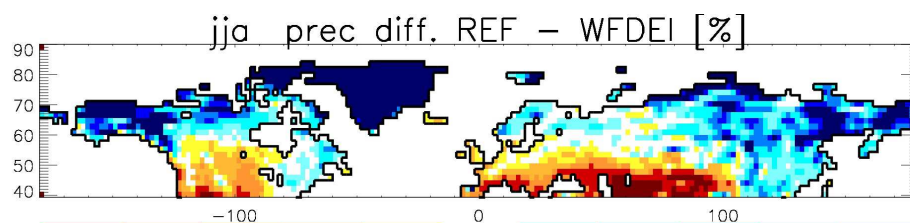
728   −110   −90   −70   −50   −30   −10   10.0   30   50   70   90   >110
729

730   **Fig. 2.**   Boreal summer (JJA) precipitation differences [%] relative to WFDEI data for a)
731   ECH6-REF, and b) ECH6-PF.
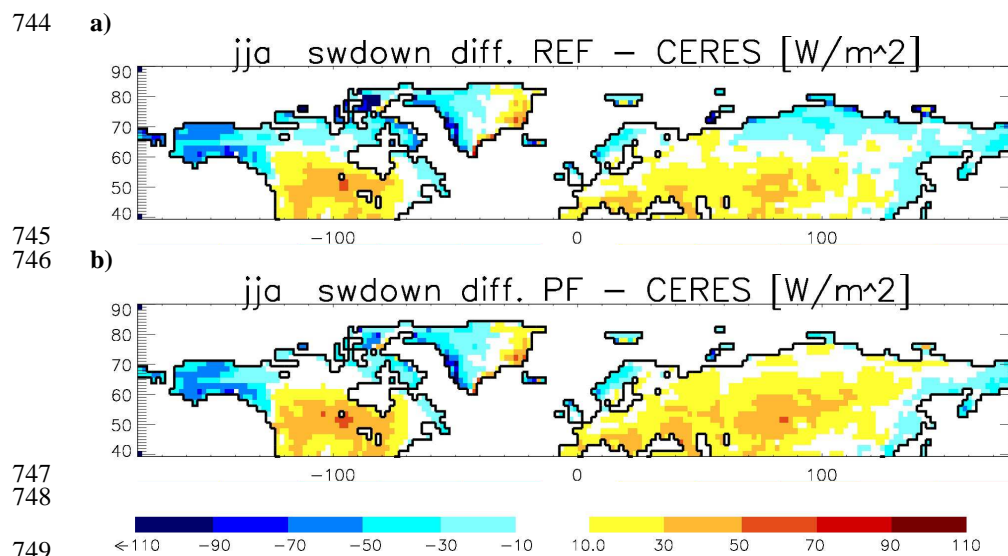
732

733

734   **a)**

735
736   **b)**

737
738

739   ≤2.5   −1.5   −0.50   0.50   1.5   2.5   3.5   4.5   5.5   6.5   7.5   8.5   > 9.5
740
741   **Fig. 3.**   Boreal summer (JJA) 2m temperature differences [K] to WFDEI data for a)
742   ECH6-REF, and b) ECH6-PF.

743

Earth System
Dynamics
Discussions

744   **a)**

745
746   **b)**

747
748

749
750
751   **Fig. 4.**   Boreal summer (JJA) surface solar incoming radiation differences [W/m²] to
752   CERES data for a) ECH6-REF, and b) ECH6-PF.

753
754

755
756
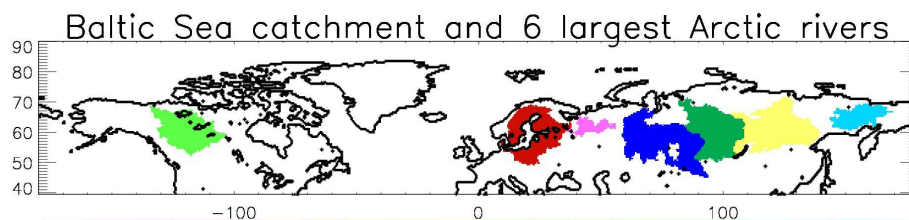
757
758
759
760   **Fig. 5.**   Catchments of the Baltic Sea and of the six largest Arctic rivers (from left to
761   right: Mackenzie, Baltic Sea, Northern Dvina, Ob, Yenisei, Lena, Kolyma).

762
763
764
765

Earth System
Dynamics
Discussions

766
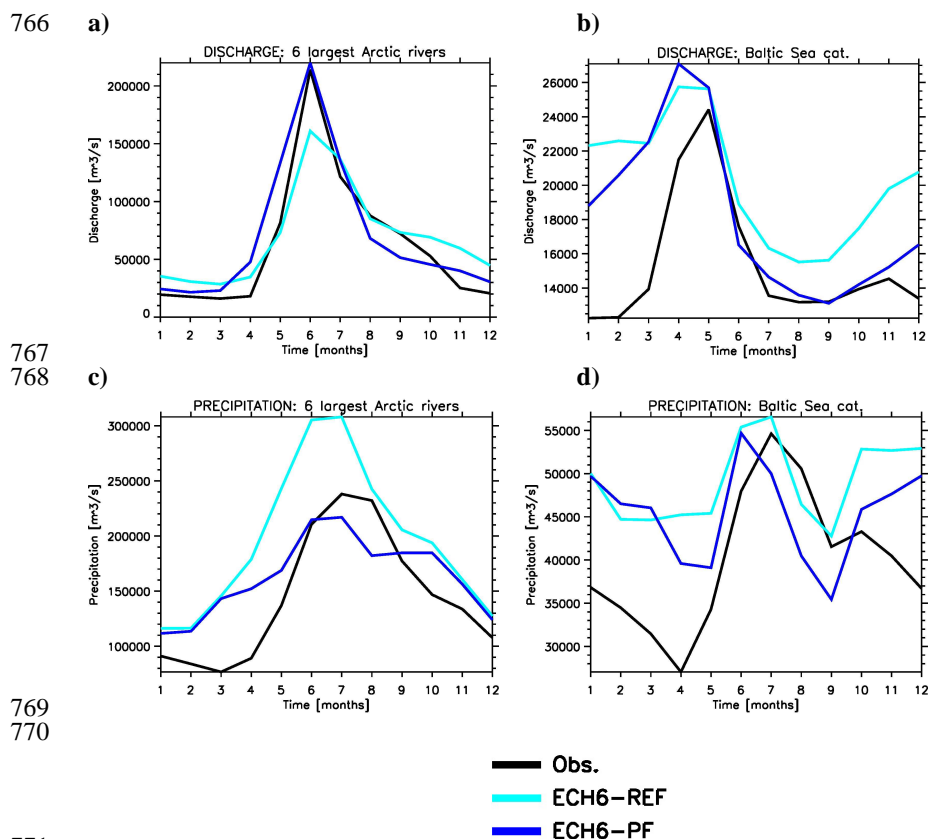
Fig. 6.   Mean monthly climatology (1989-2009) of discharge (upper panels) and
precipitation (lower panels) over the 6 largest Arctic river catchments (left column) and
the Baltic Sea catchment (land only, right column). Observations comprise climatological
observed discharge and WFDEI precipitation, respectively.
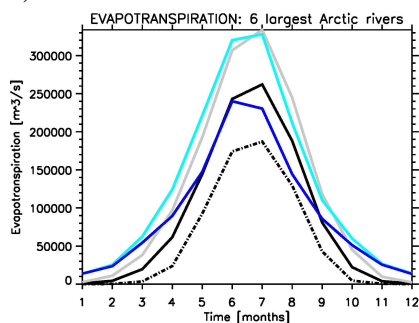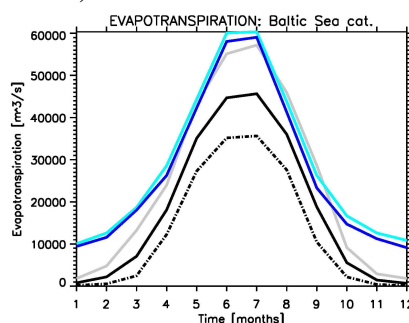
Earth System
Dynamics
Discussions

779

780

781
782

783
784

785
786
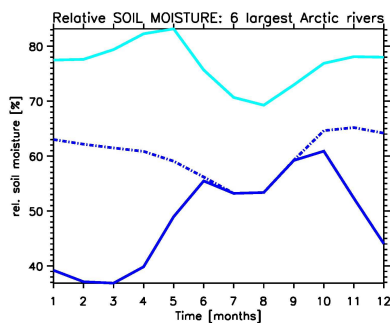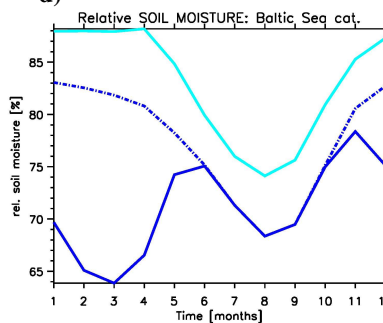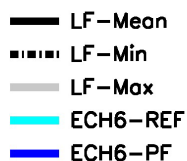
Fig. 7. Mean monthly climatology (1989-2009) of evapotranspiration (upper panels)
and relative root zone soil moisture (lower panels) over the 6 largest Arctic river
catchments (left column) and the Baltic Sea catchment (land only, right column).
Evapotranspiration data comprise the mean, minimum and maximum diagnostic estimates
from the LandFlux Eval (LF) dataset. The dashed blue line denotes the total root zone
water content (liquid + frozen) for ECH6-PF.
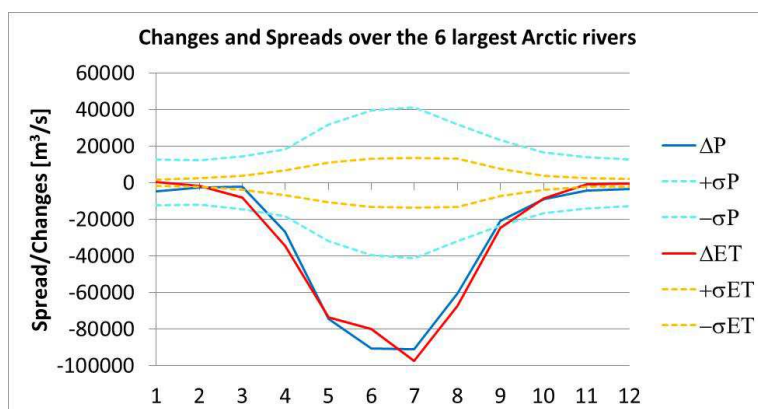
793

794

795
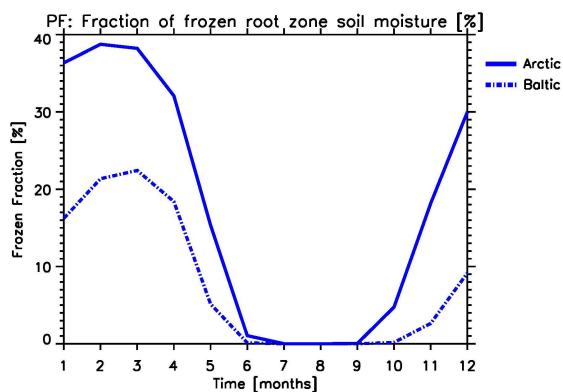
796

Fig. 8. Mean fraction of frozen root zone soil moisture (1989-2009) over the 6 largest
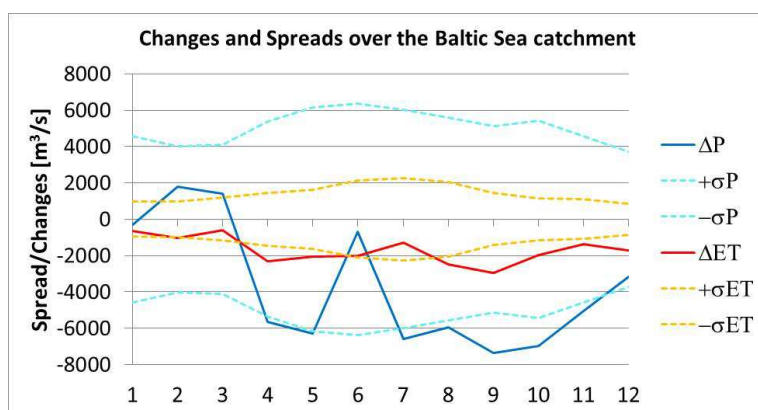Arctic river catchments (solid curve) and the Baltic Sea catchment (land only, dashed
curve).

800

801

Earth System
Dynamics
Discussions

802

803

Fig. 9.   Mean monthly climatological differences (1989-2009) of between ECH6-PF and
ECH6-REF for precipitation (*ΔP*) and evapotranspiration (*ΔET*) over the 6 largest Arctic
rivers (upper panel) and the Baltic Sea catchment (lower panel). The dashed lines indicate
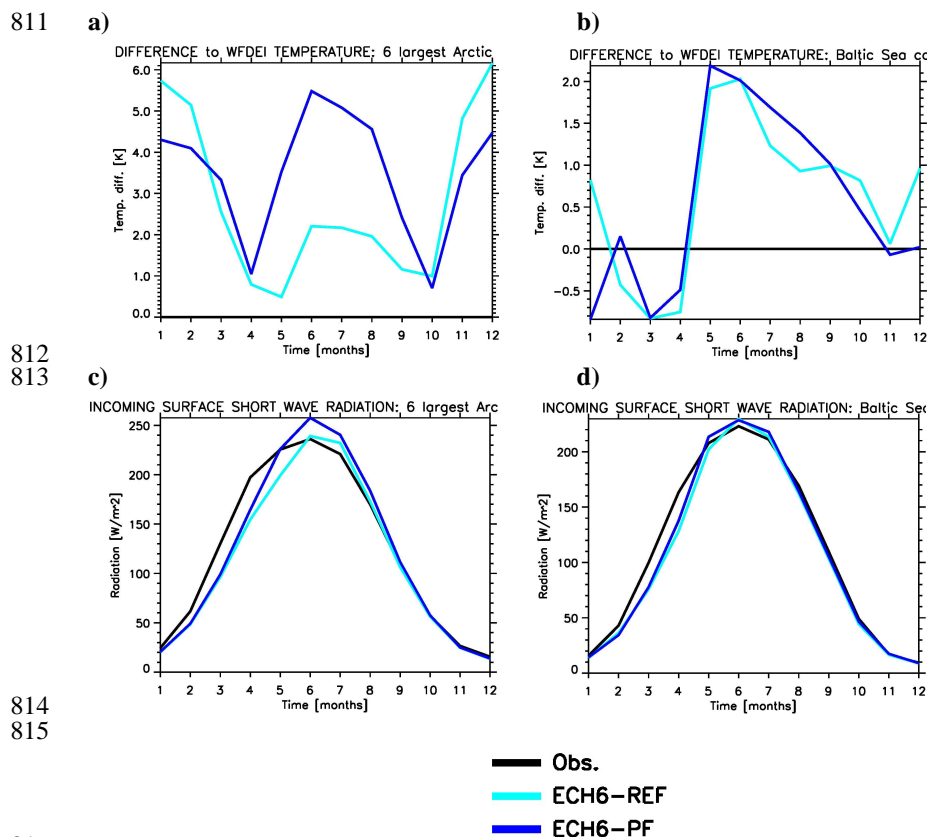the corresponding spreads obtained from MPI-ESM simulations of deVrese et al. (2016).

808

809

810

Earth System
Dynamics
Discussions

811   **a)**

812
813   **c)**

814
815

— Obs.
— ECH6-REF
— ECH6-PF

816
817
818   **Fig. 10.**   Mean monthly climatology (1989-2009) of 2m temperature differences to
819   WFDEI data (upper panels) and surface solar irradiance (SSI; lower panels) over the 6
820   largest Arctic river catchments (left column) and the Baltic Sea catchment (land only,
821   right column). SSI observations comprise CERES data for 2000-2010.

822

823

824   **a)**   **b)**

825
826   **c)**   **d)**
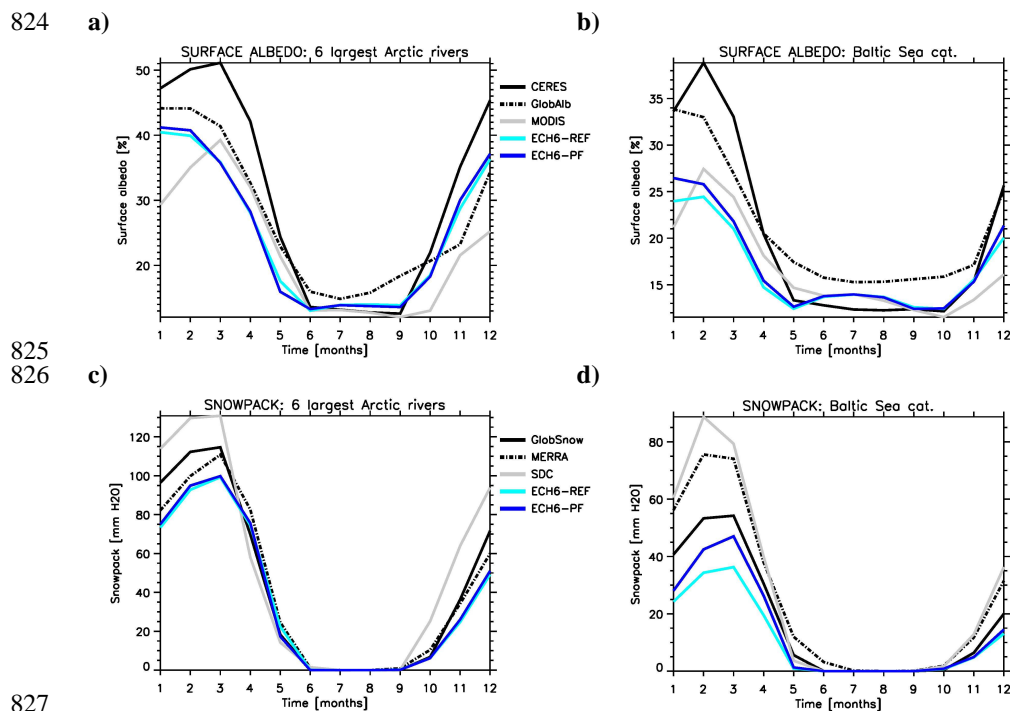

827
828
829   **Fig. 11.**   Mean monthly climatology (1989-2009) of surface albedo (upper panels) and
830   snow pack snow water equivalent (SWE; lower panels) over the 6 largest Arctic river
831   catchments (left column) and the Baltic Sea catchment (land only, right column). Albedo
832   observations data from MODIS (2000-2011), CERES (2000-2010) and GlobAlbedo
833   (1998-2011), SWE observations comprise data from GlobSnow (1989-2009), MERRA
834   (1979-2013), and SDC climatology.

835
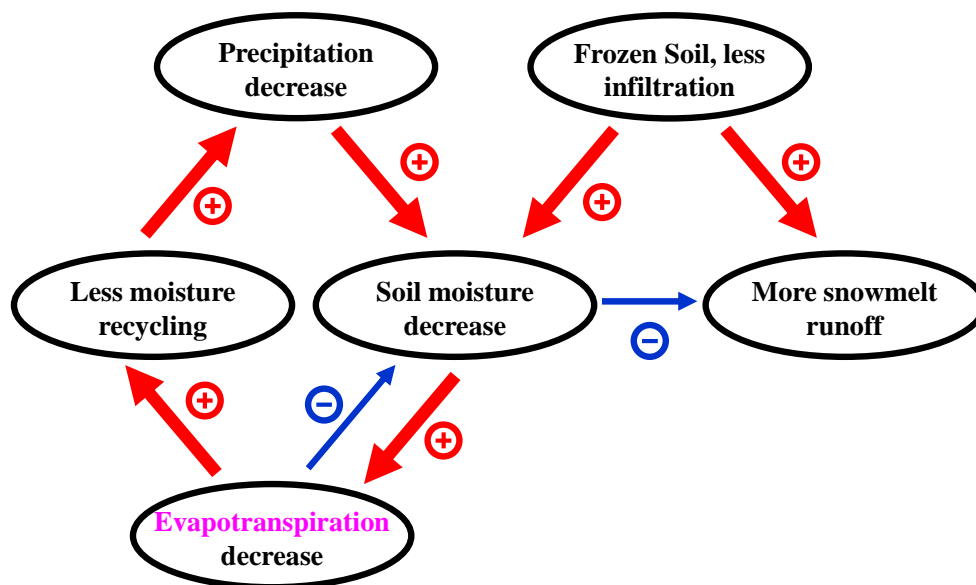
Earth System
Dynamics
Discussions

Open Access

EGU

836

837

Fig. 12. Chain of processes involved in the soil moisture precipitation feedback over high latitudes. Red arrows indicate directions supporting this feedback, blue arrows indicate compensating opposite effects.

841

842

843

844 **Table 1.** Summer (JJA) biases over the six largest Arctic rivers for 2m temperature (T_{2m}, to
845 WFDEI), radiative flux (R) into the surface due to biases in SSI (to CERES), albedo (α, to
846 GlobAlbedo) and their combined effect (comb.) as well as the estimated related impact on
847 surface temperature (T_s) and the contribution of the SSI bias to this impact.

Experiment	ΔT_{2m}	ΔR SSI	$\Delta R\ \alpha$	ΔR comb.	ΔT_s comb.	SSI cont.
ECH6-REF	2.1 K	5.0 W/m²	4.1 W/m²	9.0 W/m²	1.7 K	55%
ECH6-PF	5.0 K	15.8 W/m²	4.3 W/m²	19.8 W/m²	3.6 K	78%

848

849